AIP | Physics of Fluids

Stability and spectra of the bumpy pinch

Thomas E. Cayton and George Vahala

Citation: Physics of Fluids (1958-1988) **19**, 590 (1976); doi: 10.1063/1.861494
View online: http://dx.doi.org/10.1063/1.861494
View Table of Contents: http://scitation.aip.org/content/aip/journal/pof1/19/4?ver=pdfcov
Published by the AIP Publishing

Stability and spectra of the bumpy θ pinch

Thomas E. Cayton and George Vahala

Department of Physics, College of William and Mary, Williamsburg, Virginia 23185
(Received 3 November 1975)

Finite wavelength modes in the bumpy θ pinch are examined by performing perturbation expansions in the small bumpiness on the equations of ideal magnetohydrodynamics. The unstable modes are transverse and compressible. The evolution of two unstable classes of modes from a single unstable class is followed numerically as the plasma β is varied.

I. INTRODUCTION

The linear θ pinch is a basic prototype fusion device because of its stability to small perturbations, but since the magnetic field lines are straight there is an inherent end loss problem. To eliminate this problem the device can be made toroidal, but to achieve a (high-β) toroidal equilibrium[1] it is now necessary to superimpose both an $L=0$ axially symmetric (bumpy) and an $L=1$ helically symmetric field on the main θ-pinch field. This approach is being investigated in the (very large aspect ratio) scyllac experiment. Some of their experimental results[2] suggest that the major contribution[3] to the growth rate of the instability comes from the bumpy $L=0$ field rather than from the stronger helical $L=1$ field, thus giving some continuing importance to examining the bumpy θ pinch—a problem first considered by Haas and Wesson[4] in 1967. The bumpy θ pinch is also of some interest because in any confinement scheme some axial inhomogeneities (due to discrete coil windings) are unavoidably introduced in the applied vacuum fields.

Haas and Wesson[4] considered the long-wavelength stability using a thin skin sharp boundary model (we introduce the small quantity δ to parametrize the bumpiness of the field lines and let k be the corresponding wavenumber. In the long wavelength case $k \equiv \epsilon \ll \delta$). They found that for sufficiently high β the $m=1$ mode was stabilized (wall stabilization). Weitzner,[3] and Freidberg and Marder[5] considered the more realistic diffuse profile mode, assuming a Gaussian pressure profile, and in their long wavelength analyses found no sign of wall stabilization on the $m=1$ growth rates, even up to $\beta=0.95$. Furthermore, they both[3,5] showed the existence of unstable modes through a δW analysis, no matter where the conducting wall is positioned. This apparent paradox was resolved by these authors[6] who considered a sharper diffuse pressure profile. It was found[6] that the $m=1$, $n=0$ (n gives the number of radial nodes in the eigenfunction) mode was, for sufficiently high β, wall stabilized, in agreement with the sharp boundary result,[4] but higher n unstable modes were also found which were not wall stabilized, in agreement with their δW analysis.[3,5] The resultant non-Sturmian modal structure was quite complicated and was explained by a spectral analysis developed by Weitzner.[6]

In these long wavelength calculations,[3,4,6] double perturbation expansions are performed, first in ϵ then in δ. This corresponds to what is termed the "new ordering" in helical calculations,[7] $\epsilon \ll \delta \leqslant 1$.

In this paper we consider the finite wavelength bumpy θ pinch by expanding only in the small bumpiness parameter δ, with the wavenumber $k=O(1)$ in δ. This, in helical calculations,[8–11] corresponds to the "old ordering": $\delta \ll k \leqslant 1$. The comparison of stability between finite and long wavelength modes is marred by ambiguities because of the sensitiveness of the finite wavelength equilibria on wall position and k, (see Fig. 1). Hence, most of our attention is focused on the spectral properties of the finite wavelength modes.

Before summarizing the results of this paper, we must stress that, in what follows, the terms compressibility and incompressibility refer only to the two-dimensional transverse velocity $\vec{u}=u_r\hat{r}+u_\theta\hat{\theta}$, and not to the full three-dimensional flow $\mathbf{u}_1=\vec{u}+u_z\hat{z}$. In fact, it is shown in the appendix that the flow $\mathbf{u}_1$ is incompressible in the finite wavelength case while $\vec{u}$ is compressible. (It should be remarked that the longitudinal component of flow u_z plays no explicit role in the properties of the transverse modes and so the concept of compressibility or incompressibility for the two-dimensional transverse flow is meaningful.)

In Sec. II we present the finite wavelength equilibria, which can no longer be obtained analytically as in the long wavelength case,[3] while in Sec. III we outline the stability calculation. It is again found, as in all the other problems in which this perturbation procedure has been employed (both in straight[3,6,12,13] and toroidal[14,15] systems, and even in guiding-center plasma models[16–18]) that the unstable modes: (i) have frequency $\omega \approx k\delta$, (ii) have flow principally across the magnetic field, the transverse modes, and (iii) are found by numerical solution of ordinary differential equations which explicitly exhibit the stable Alfvén continuum (or its trivial generalization in guiding-center plasma theory[17,18]).

The normalized growth rates are plotted for various wall positions and pressure profiles and are contrasted with the long-wavelength normalized growth rates (it is to be stressed that no comparison is being made between actual growth rates as to whether the finite or the long-wavelength modes are more stable or unstable). It is found that the finite wavelength modes are compressible while for the long-wavelength case the modes are incompressible (this is also true in the guiding center plasma model[17,18]). Moreover, employing the additional constraint of incompressibility on the finite-wavelength modes seems to lead to a null eigenvalue problem for this constrained set of ordinary differential equations. The boundary conditions are that the plasma extends to a rigid perfectly conducting wall and regularity on axis

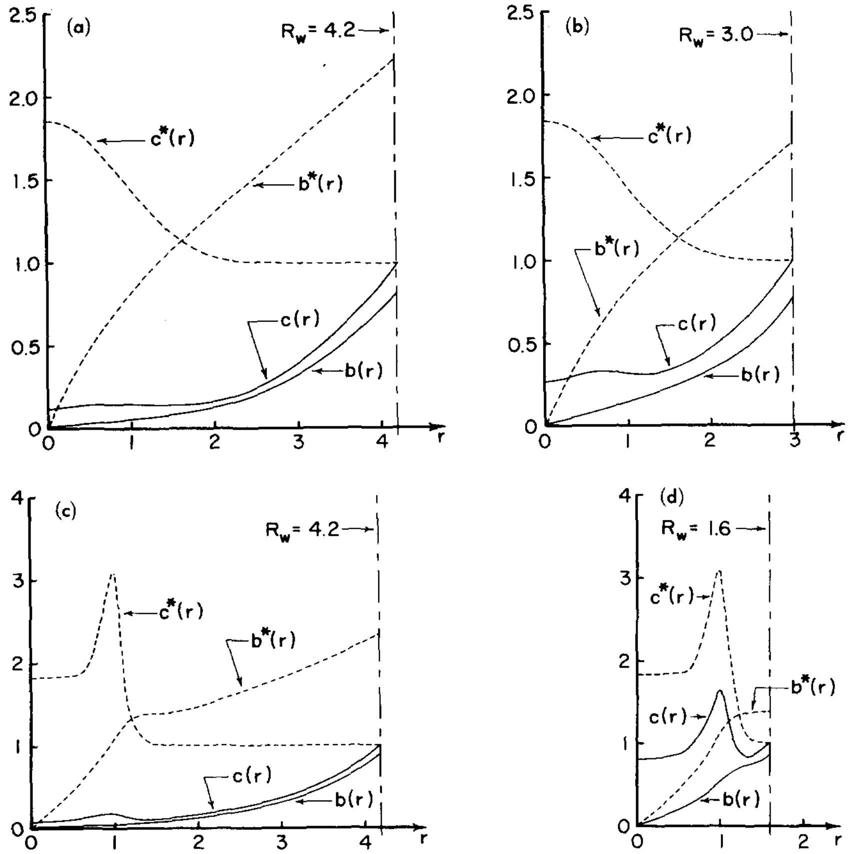

FIG. 1. Typical subsidary fields ($\beta = 0.7$) for finite-wavelength (solid curves) and long wavelength (dashed curves) equilibria for two wall positions: The Gaussian pressure profile with (a) $r_w = 4.2$; (b) $r_w = 3.0$; the sharp profile with (c) $r_w = 4.2$; (d) $r_w = 1.6$. Note the dependence of the finite-wavelength fields on wall position.

($r = 0$).

Following Weitzner's spectral analysis[6,19] it is found that for sufficiently high β, there should be a transition from a set of {1 unstable class} to a set of {2 unstable classes, 1 stable class}, each class of modes accumulating at $\omega = 0$ (this is also true for the long wavelength case, see Sec. IV). Numerically, Freidberg *et al.*[6] did not find the unstable class of modes localized on the outside of the plasma. However, for the finite-wavelength case, we have found both classes of unstable modes as well as the stable class. The evolution in β of the 2 unstable classes (one localized inside, the other localized outside the plasma) from the original unstable class (localized on the outside) is presented in Sec. IV. We note that the radial localization of these modes is as predicted by theory.[6,19]

II. FINITE-WAVELENGTH EQUILIBRIA

We consider straight, static, axially symmetric, magnetohydrodynamic equilibria assuming currents flow only in the ignorable direction. We employ standard cylindrical polar coordinates and use appropriate dimensionless variables.[3] Under these circumstances, the equilibria equations are reduced to a nonlinear elliptic partial differential equation for $\psi(r, z)$:

$$\frac{1}{r}\frac{\partial}{\partial r}\left(\frac{1}{r}\frac{\partial \psi}{\partial r}\right)+\frac{1}{r^2}\frac{\partial^2 \psi}{\partial z^2} = -p'(\psi)\ , \tag{1}$$

where ψ is the magnetic stream function so that

$$B_r(r, z) = \frac{1}{r}\frac{\partial \psi}{\partial z}\ , \quad B_z(r, z) = -\frac{1}{r}\frac{\partial \psi}{\partial r}\ . \tag{2}$$

Primes denote differentiation with respect to the argument.

We restrict our attention to a particular class of equilibria with small bumpiness in the field lines by assuming

$$\psi(r, z) = \psi_0(r) + \delta\psi_1(r)\cos(kz) + O[\delta^2\cos(2kz)]\ , \tag{3}$$

where δ measure the bumpiness while k is the wavenumber of the bumps. For finite-wavelength equilibria, $k = O(1)$ in δ. The equilibrium magnetic field is, from Eq. (2) and (3)

$$\begin{aligned} &B_r(r, z) = \delta k b(r)\sin(kz) + O(\delta^2)\ , \quad B_\theta(r, z) \equiv 0\ , \\ &B_z(r, z) = a(r) + \delta c(r)\cos(kz) + O(\delta^2)\ , \end{aligned} \tag{4}$$

where $ra = -\psi_0'(r)$, $rb = -\psi_1(r)$ and

$$rc(r) = [rb(r)]' = -\psi_1'(r)\quad . \tag{5}$$

On substituting Eq. (3) into Eq. (1) we obtain a set of linear ordinary differential equations for ψ_0, $\psi_1, \ldots,$ so that

$$O(1):\quad p(r) + \tfrac{1}{2}a^2(r) = \tfrac{1}{2}\ , \tag{6}$$

$$O(\delta):\quad \psi_1''(r) - \frac{1}{r}\psi_1'(r) - \left[k^2 + \frac{r}{a}\left(\frac{a'}{r}\right)'\right]\psi_1(r) = 0\ , \tag{7}$$

where in Eq. (6) we have assumed the plasma to extend to a perfectly conducting rigid wall and normalized so that $a(r_w) = 1$. The boundary conditions for Eq. (7) are $\psi_1(0) = 0$ and $\psi_1'(r_w)/r_w = -1$. The first condition arises from the requirement that B_r be regular at $r = 0$ while the second condition arises from our normalization: We normalize so that the applied $l = 0$ helical field $c(r)$ is such that $c(r_w) = 1$. Equation (7) can be rewritten, using

Eq. (5), in the form

$$O(\delta):\ (ac-a'b)'=k^2 ab\ . \tag{8}$$

For a given pressure profile $p(r)$, Eq. (6) determines the basic θ-pinch field $a(r)$, while the subsidiary fields $b(r)$ and $c(r)$ are determined by solving the boundary value problem for ψ_1. Since Eq. (7) is a linear homogeneous equation for ψ_1, the functional form will not change with different wall positions. However, the $\psi_1(r)$ themselves can differ by scalar multiples for various r_w positions. Indeed, for both the Gaussian

$$p_G(r)=\tfrac{1}{2}\beta\exp(-r^2) \tag{9}$$

and sharp pressure profiles[6]

$$p_s(r)=\frac{\beta}{2}\frac{1-\tanh[3(r^2-1)]}{1+\tanh(3)}\ , \tag{10}$$

the finite-wavelength equilibria are affected by different wall positions while the long wavelength equilibria are not. This is shown in Fig. 1. In the long-wavelength case, denoted by *, $O(k)\ll O(\delta)$ so that Eq. (8) would become

$$a^*(r)\,c^*(r)-a'^*(r)\,b^*(r)=1\ , \tag{8*}$$

since $c^*(r_w)=1$ by normalization. Thus, for various wall positions in the region $a^*=1$ (i.e., $p^*=0$) the c^* field is totally unaffected by the particular wall position.

III. STABILITY AND GROWTH RATES FOR THE TRANSVERSE MODES

If one differentiates the linearized equations of ideal magnetohydrodynamics in time and then takes the Laplace transform in time [$\exp(i\overline{\omega}t)$, with $\mathrm{Im}\,\overline{\omega}<0$], then[3,12]

$$-p_0\overline{\omega}^2\mathbf{u}_1+\nabla P=\mathbf{T}\ , \tag{11}$$

where

$$\begin{aligned} P&\equiv i\overline{\omega}(p_1+\mathbf{B}_0\cdot\mathbf{B}_1)\ ,\\ \mathbf{T}&\equiv(i\overline{\omega}\mathbf{B}_1\cdot\nabla)\mathbf{B}_0+(\mathbf{B}_0\cdot\nabla)\,i\,\overline{\omega}\,\mathbf{B}_1 \end{aligned} \tag{12}$$

can be expressed in terms of the perturbed velocity $\mathbf{u}_1$. Subscripts 0 and 1 refer to equilibrium and perturbed quantities, respectively. The arrow ($\vec{\ }$) over a vector will denote the r,θ component vector:

$$\begin{aligned} \mathbf{u}_1&=\vec{\mathbf{u}}+u_z\hat{z}=u_r\hat{r}+u_\theta\hat{\theta}+u_z\hat{z}\ ,\\ \vec{\nabla}\cdot\vec{\mathbf{u}}&=\frac{1}{r}\frac{\partial}{\partial r}(ru_r)+\frac{1}{r}\frac{\partial u}{\partial\theta}\ . \end{aligned} \tag{13}$$

It is again found that the unstable modes are those with flow principally across the magnetic field

$$\begin{aligned} u_r(r,\theta,z,t)&=i\exp(im\theta+il\delta kz)\\ &\quad\times\exp(i\delta k\omega t)\,[u_r^0(r)+\delta u_r^1(r)\cos(kz)+O(\delta^2)]\ ,\\ u_\theta(r,\theta,z,t)&=\exp(im\theta+il\delta kz)\\ &\quad\times\exp(i\delta k\omega t)\,[u_\theta^0(r)+\delta u_\theta^1(r)\cos(kz)+O(\delta^2)]\ ,\\ u_z(r,\theta,z,t)&=O(\delta)\ ; \end{aligned} \tag{14}$$

that is, low frequency, $\overline{\omega}=O(\delta)$, long-wavelength [of $O(\delta^{-1})$] transverse modes. It is convenient to define

$$D^{0,1}\equiv\frac{1}{r}[(ru_r^{0,1})'+m\,u_\theta^{0,1}]\ . \tag{15}$$

From Eqs. (11) and (12) we find

$$\vec{\nabla}P=0+O(\delta)\ , \tag{16}$$

so that

$$O(1):\ D^0(r)=0\ . \tag{17}$$

Thus, to leading order in δ, the flow is incompressible. [In the long-wavelength case,[3] this procedure yields that $\vec{\mathbf{u}}$ is incompressible to all orders in δ.] On taking the curl of Eq. (11) we have

$$\nabla\times\mathbf{T}=0+O(\delta^2)\ . \tag{18}$$

The r component of Eq. (18) yields [at $O(\delta)$]

$$O(\delta\sin kz):\ D^1=-k^2\frac{r}{am}\left(y_2+\frac{m^2}{r^2}b\chi_0\right)\ , \tag{19}$$

while the z component yields

$$O(\delta\cos kz):\ y_2'=-\frac{y_2}{r}\left(1+\frac{ra'}{a}\right)+\frac{m^2}{r^2}\left(y_1-2\frac{a'b}{a}\chi_0\right)\ , \tag{20}$$

where (since $D^0=0$)

$$ru_r^0\equiv m\chi_0(r)\ ,\quad u_\theta^0\equiv-\chi_0'(r)\ , \tag{21}$$

and $y_1(r)$ and $y_2(r)$ are defined by

$$\begin{aligned} y_1&\equiv-\frac{ar}{m}u_r^1+b\chi_0'-\Delta\chi_0\ ,\\ y_1'&\equiv\frac{a'}{a}y_1+y_2+\left(\frac{a'}{a}\Delta-\Delta'\right)\chi_0-\frac{ar}{m}D^1, \end{aligned} \tag{22}$$

and the equilibrium quantity Δ,

$$\Delta(r)\equiv c-a'b/a\ . \tag{23}$$

We note that this mode is compressible, $D^1(r)\neq0$. Finally, from the z component of the curl of Eq. (11)

$$\begin{aligned} O(\delta^2):\ &\frac{1}{r}[r\chi_0'(\rho_0\omega^2-l^2a^2)]'-\frac{m^2}{r^2}\chi_0(\rho_0\omega^2-l^2a^2)\\ &=\frac{1}{2}\left[\left(\frac{a'}{a}\Delta-\Delta'\right)y_2+\frac{a'}{a}\frac{m^2b}{r}\right.\\ &\quad\left.\times\left\{2y_1+\chi_0\left(3\Delta-2\frac{b}{r}-\frac{a}{a'}\Delta'\right)\right\}-\frac{m}{r}abD^1\right]\ . \end{aligned} \tag{24}$$

Since the plasma extends to the conducting wall $\mathbf{n}\cdot\mathbf{u}_1=0$, i.e.,

$$\begin{aligned} O(1):&\ \chi_0(r_w)=0\ ,\\ O(\delta):&\ y_1(r_w)=0\ . \end{aligned} \tag{25}$$

In the long-wavelength case,[3] $O(k)\ll O(\delta)$, Eq. (19) would become

$$D^{*1}=0\ , \tag{19*}$$

and the equilibrium quantity Δ^*, from Eqs. (23) and (8*),

$$\Delta^*=1/a^*\ . \tag{23*}$$

It is then found that the eigenvalue problem, Eqs. (24), (20), and (22), reduce to that considered by Weitzner.[3]

The eigenvalue problem, Eqs. (24), (20), and (22) is a fourth-order set of ordinary differential equations

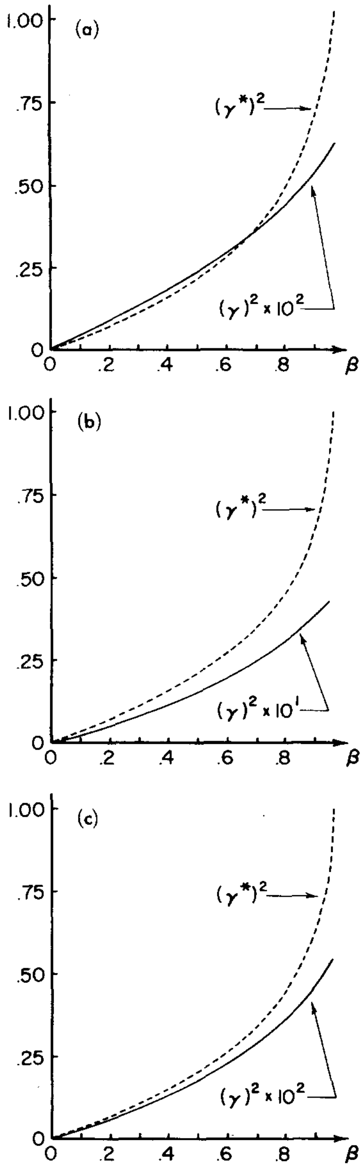

FIG. 2. Normalized growth rate squared versus β for the least stable mode for Gaussian profile in finite wavelength (solid) and long-wavelength (dashed) cases with (a) $r_w = 4.2$; (b) $r_w = 3.0$; (c) is for $r_w = 3.0$ but with renormalized equilibria so that the fields are unaffected by wall position. Wall stabilization occurs as predicted by a δW analysis.

with two regularity conditions at the origin and two homogeneous boundary conditions at the wall. From Eq. (24) we also find the Alfvén continuum,

$$\omega^2 = l^2 [a^2(r)/\rho_0(r)] . \tag{26}$$

A. Growth rates

Numerically, we recover the long-wavelength unstable modes of Weitzner[3] by setting $k \simeq 10^{-6}$ in our eigenvalue equations (19) and (8) since numerically $D^1 \simeq k^2$ and $\Delta - \Delta^* \sim k^2$ (in fact, even for $k = 0.15$ one recovers Weitzner's growth rates to within 20%). In the results below we have set $k = 1$ when considering the finite-wavelength modes. In Fig. 2 we plot the normalized growth rate squared

$$\gamma^2 = -\omega^2 = -(\overline{\omega}^2/k^2\delta^2)$$

versus β for the $m=1$, $l=0$ mode for the wall positions $r_w = 4.2$ and $r_w = 3$, assuming the Gaussian pressure profile, Eq. (9). The dashed curves are the analogous normalized growth rates $\gamma^{*2} = -\overline{\omega}^2/\epsilon^2\delta^2$ [with $k \to \epsilon$, $O(\epsilon) \ll O(\delta)$] for the long wavelength case. In Fig. 2(b) we have normalized so that $c(r_w) = 1$ when $r_w = 3$, cf. Fig. 1(a), while in Fig. 2(c) we have chosen the normalization that the applied $l = 0$ helical field $c(r)$, have the same value at $r = 0$ (on axis) irrespective of wall position. Notice that the growth rates, with this normalization, are slightly stabilized by the closer wall position, this is in agreement with the general argument based on δW analysis.

In Fig. 3 we plot γ^2 and γ^{*2} versus β for the sharp profile, Eq. (10), but keeping (as we will for the remainder of this paper) the normalization $c(r_w) = 1$ for various wall positions. Note that for distant wall positions, the finite-wavelength $n = 0$ mode is not wall stabilized [Fig. 3(a)]. However, wall stabilization does occur for close wall positions, but only for extremely high β [Fig. 3(b)].

It should be noted that if we add the equation $D^1(r) \equiv 0$, the incompressibility condition, rather than Eq. (19), to the set of Eqs. (20), (22), and (24), then we seem to have a null eigenvalue problem. If we impose the incompressibility constraint on Eqs. (19), (20), (22), and (24), i.e., $y_2 \equiv -(m^2/r^2) b\chi_0$ in addition to $D^1 \equiv 0$, then the system reduces to a single second-order equation involving only χ_0, but this also seems to be a null eigenvalue problem.

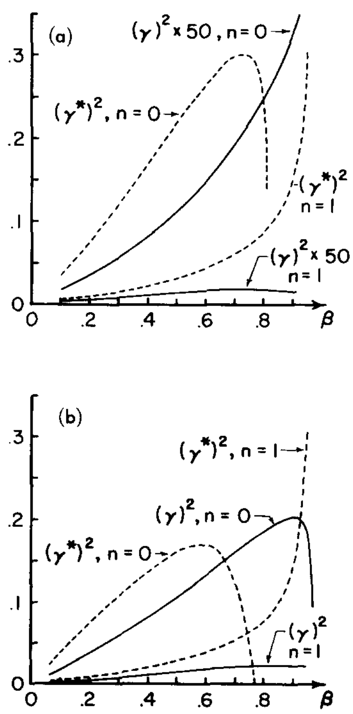

FIG. 3. Normalized growth rate squared versus β for modes for the sharp profile with (a) $r_w = 4.2$; (b) $r_w = 1.6$. Note that the mode with $n = 0$ radial nodes is stabilized for sufficiently high β while the other modes are not stabilized.

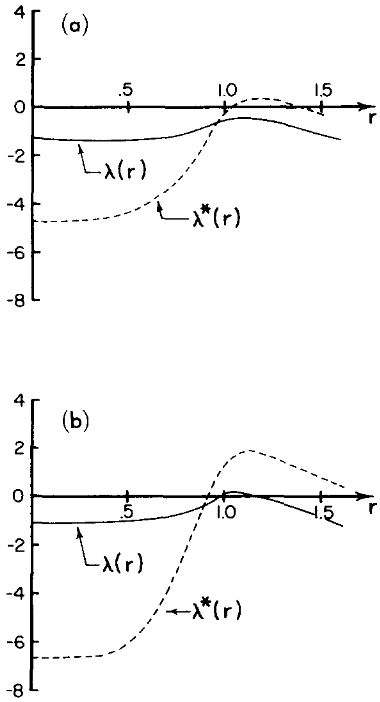

FIG. 4. $\lambda(r)$ for the finite-wavelength (solid) and long-wavelength (dashed) cases for (a) $\beta=0.9$; (b) $\beta=0.95$.

IV. SPECTRAL PROPERTIES OF THE TRANSVERSE MODES $l=0$

For $l=0$, the Alfvén continuum $\omega^2=l^2a^2(r)/\rho_0(r)$ degenerates to the point $\omega^2=0$, which is an accumulation point for the spectrum. To investigate the behavior of the solutions around $\omega^2=0$ we follow Weitzner's analysis[6,19] by looking for rapidly varying eigenfunctions localized about $r=r_0$. Introducing the small parameter ϵ_1, which measures the localization of these modes

$$r-r_0=\epsilon_1\,\mathcal{E},\quad \mathcal{E}=O(1) \text{ in } \epsilon_1\,,$$

we have, from Eqs. (20), (22), and (24),

$$\frac{d}{dr}\sim\epsilon_1^{-1}\,,\quad \omega=\epsilon_1\,\omega_1\,,\quad y_1\sim\epsilon_1\,,\quad y_2\sim\epsilon_1\,.$$

Hence, to leading order

$$\rho_0(r_0)\,\omega_1^2\,\chi_0''(\mathcal{E})+\frac{m^2}{r_0^2}\,\frac{a'(r_0)\,b(r_0)}{a(r_0)}\,\lambda(r_0)\,\chi_0(\mathcal{E})=0\,, \tag{27}$$

where

$$\lambda(r)\equiv[b(r)/r]-2\Delta(r)\,. \tag{28}$$

From Eq. (27) we see that for $\lambda(r)>0$, oscillatory solutions are possible if $\omega^2>0$, thus, $\omega^2=0$ is a point of accumulation of the spectrum from the stable side. For

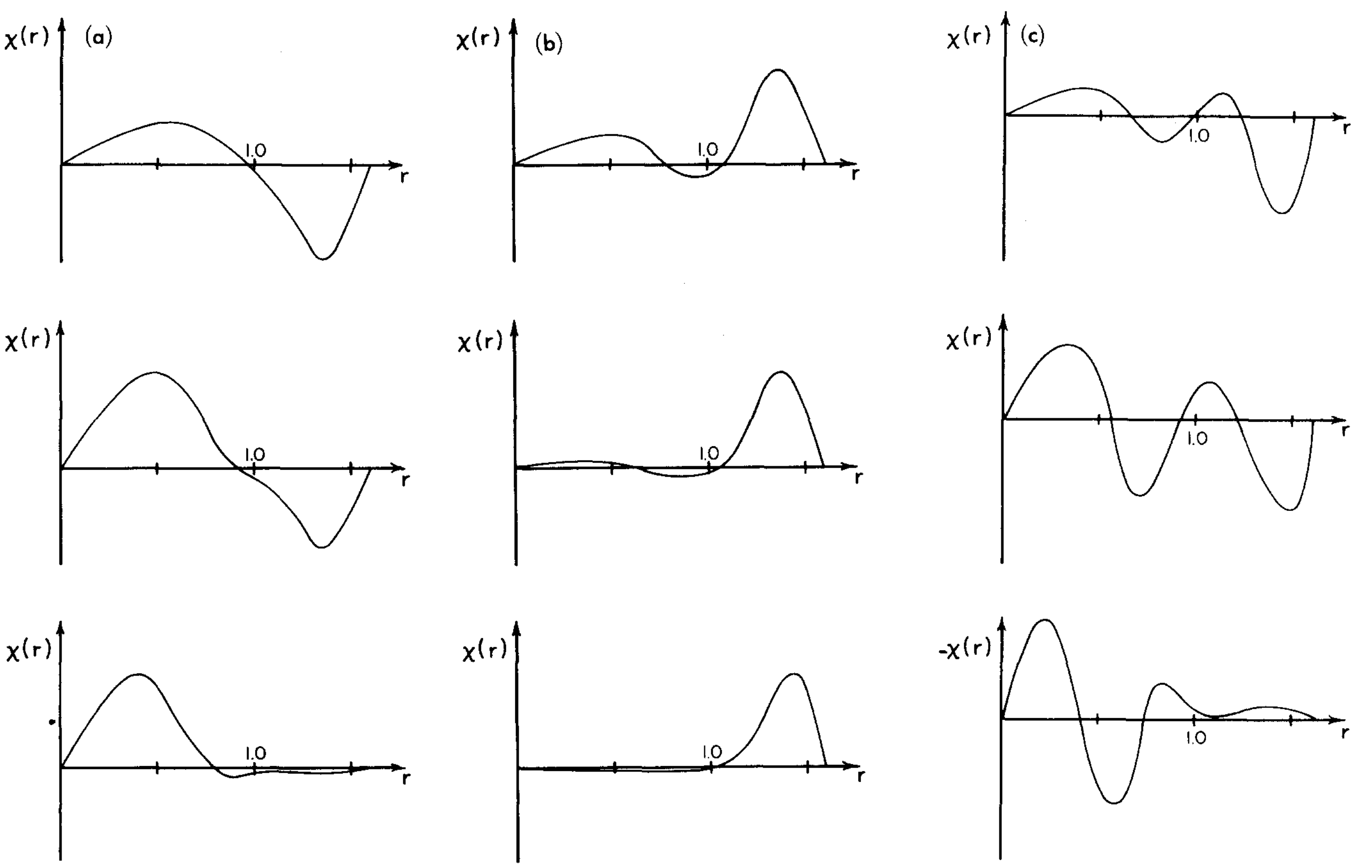

FIG. 5. Evolution of unstable eigenfunctions of the finite-wavelength case as β varies, following $-\omega^2$ trajectories similar to those shown in Fig. 3(b). The eigenvalue corresponding to an eigenfunction with 1 radial node is followed in (a); 2 nodes in (b); 3 nodes in (c). There is only one eigenfunction with 0, 1, 2, or 3 nodes for the lowest β value (top); for the highest β (bottom) there are two different unstable eigenvalues corresponding to eigenfunctions with 1 node [see (a), (b)]. These two eigenfunctions have different localization. Similar behavior was also observed for other numbers of radial nodes.

eigenvalues very close to zero, the corresponding eigenfunctions are expected to be localized in the regions in r where $\lambda(r) > 0$. For $\lambda(r) < 0$ then, $\omega^2 = 0$ is a point of accumulation of the spectrum from the unstable side with similar localization of the eigenfunctions. [It should be noted that for the long-wavelength case,[1] $\lambda \to \lambda^*$ with λ^* given by Eq. (28) with $a \to a^* = a$, $b \to b^*$, $\Delta \to \Delta^* = 1/a^*$.]

In Fig. 4 we plot λ and λ^* for $\beta = 0.90$ and $\beta = 0.95$ using the sharp pressure profile, Eq. (10). For the long-wavelength case one sees that for $\beta = 0.90$ there should be 2 unstable classes of modes (localized on the inside and outside of the plasma) and 1 stable class of modes (localized near the outside of the plasma). As β increases the unstable class of modes localized outside the plasma disappears. In the numerical computations of Freidberg *et al.*,[6] this externally localized unstable class was never found. For the finite-wavelength case, we find that for $\beta < 0.94$ there is only one class of unstable modes while for $\beta \geq 0.95$ we find numerically both externally and internally localized unstable modes as well as one stable class of modes, in agreement with Weitzner's theory (see Fig. 4). In Fig. 5 we show the eigenfunction behavior for various β. For a particular β we show the $n = 1$, 2, and 3 eigenfunctions in Figs. 5(a), 5(b), and 5(c), where n is the number of radial modes. They are unstable and all localized on the outside of the plasma. As β increases, we follow the ω^2 trajectories and see:

(i) [Fig. 5(a)] The $n = 1$ *externally* localized modes becomes an $n = 1$ *internal* mode.

(ii) [Fig. 5(b)] The $n = 2$ *externally* localized mode loses a node and becomes an $n = 1$ *external* mode. This gives rise to a second class of unstable modes.

(iii) [Fig. 5(c)] The $n = 3$ *externally* localized mode loses a node and becomes an $n = 2$ *internal* mode.

We also find stable eigenfunctions for the highest β values. The mode with $n = 1$ nodes appears before the $n = 0$ mode (this has also been seen by Freidberg *et al.*[6]).

ACKNOWLEDGMENT

The authors are grateful to Harold Weitzner for valuable discussions and comments.

The authors also wish to thank J. P. Freidberg for pointing out to us that the full flow velocity is incompressible.

APPENDIX: COMPRESSIBILITY AND INCOMPRESSIBILITY

In Sec. III it was shown that the transverse flow $\vec{u}$ is *compressible*, i.e., from Eqs. (13)–(15) and (19),

$$\vec{\nabla} \cdot \vec{u} = i \exp(iA) [\delta D^1(r) \cos kz + O(\delta^2)] = 0 + O(\delta) , \tag{A1}$$

where $A \equiv m\theta + l\delta kz + \delta k\omega t$.

In this appendix we show that the full velocity $\mathbf{u}_1 = \vec{u} + u_z \hat{z}$ is *incompressible*, i.e., $\nabla \cdot \mathbf{u}_1 = 0 + O(\delta^2)$. To do this, we must now assume an explicit expression for u_z [see Eq. (14)]. Compatibility requirements give

$$u_z(r, \theta, z, t) = i \exp(iA) [\delta u_z^1(r) \sin kz + O(\delta^2)] . \tag{A2}$$

From the equation of motion (11), with modes $\bar{\omega} = O(\delta)$, we see that

$$\nabla P = \mathrm{T} + O(\delta^2) , \tag{A3}$$

where [since $D^0 = 0$, Eq. (17)]

$$\begin{aligned} T_r &= k^2 \delta \exp(iA) \frac{im}{r} \left(y_1 - \frac{2a'b}{a} \chi_0 \right) \cos kz + O(\delta^2) , \\ T_\theta &= -k^2 \delta \exp(iA)\, a y_2 \cos kz + O(\delta^2) , \\ T_z &= -k^3 \delta \exp(iA) \frac{ir}{m} a y_2 \sin kz + O(\delta^2) , \\ P &= -\gamma p \nabla \cdot \mathbf{u}_1 - k^2 \delta \exp(iA) \frac{ir}{m} a y_2 \cos kz + O(\delta^2) , \end{aligned} \tag{A4}$$

with the full (three-dimensional) divergence

$$\nabla \cdot \mathbf{u}_1 \equiv i\delta \exp(iA) (D^1 + k u_z^1) \cos kz + O(\delta^2) . \tag{A5}$$

It is immediately seen from the θ component of Eq. (A3) and from Eqs. (A4) and (A5) that for $m \neq 0$,

$$\nabla \cdot \mathbf{u}_1 = 0 + O(\delta^2) . \tag{A6}$$

[1]A. A. Blank, H. Grad, and H. Weitzner, in *Plasma Physics and Controlled Nuclear Fusion Research* (International Atomic Energy Agency, Vienna, 1969), Vol. II, p. 607.
[2]S. C. Burnett, W. R. Ellis, C. F. Hammer, C. R. Harder, H. W. Harris, F. C. Jahoda, W. E. Quinn, A. S. Rawcliffe, F. L. Ribe, G. A. Sawyer, R. E. Siemon, K. S. Thomas, and F. L. Zimmerman, in *Plasma Physics and Controlled Nuclear Fusion Research* (International Atomic Energy Agency, Vienna, 1971), Vol. III, p. 201.
[3]H. Weitzner, Phys. Fluids **16**, 237 (1973).
[4]F. Haas and J. Wesson, Phys. Fluids 10, 2245 (1967).
[5]J. P. Freidberg and B. M. Marder, Phys. Fluids **16**, 247 (1973).
[6]J. P. Freidberg, B. M. Marder, and H. Weitzner, Nucl. Fusion **14**, 809 (1974).
[7]H. Weitzner, Phys. Fluids **14**, 658 (1971).
[8]H. Grad and H. Weitzner, Phys. Fluids 12, 1725 (1969).
[9]M. N. Rosenbluth, J. L. Johnson, J. M. Greene, and K. E. Weimer, Phys. Fluids 12, 726 (1969).
[10]F. L. Ribe and M. N. Rosenbluth, Phys. Fluids **13**, 2572 (1970).
[11]J. Nuhrenberg, Phys. Fluids **13**, 2082 (1970).
[12]G. Vahala, Phys. Fluids **17**, 1449 (1974).
[13]T. E. Cayton and G. Vahala, Plasma Phys. (to be published).
[14]G. Vahala, Phys. Fluids 18, 1034 (1975).
[15]J. A. Tataronis, W. Grossmann, and H. Weitzner, Plasma Phys. (to be published).
[16]H. Weitzner, Phys. Fluids **19**, 000 (1976).
[17]M. J. Schmidt and G. Vahala, Plasma Phys. (to be published).
[18]G. Vahala and L. Vahala, Bull. Am. Phys. Soc. 20, 1357 (1975).
[19]H. Weitzner (private communication).